DISCLAIMER

This report was prepared as an account of work sponsored by an agency of the United States Government. Neither the United States Government nor any agency thereof, nor any of their employees, makes any warranty, express or implied, or assumes any legal liability or responsibility for the accuracy, completeness, or usefulness of any information, apparatus, product, or process disclosed, or represents that its use would not infringe privately owned rights. Reference herein to any specific commercial product, process, or service by trade name, trademark, manufacturer, or otherwise does not necessarily constitute or imply its endorsement, recommendation, or favoring by the United States Government or any agency thereof. The views and opinions of authors expressed herein do not necessarily state or reflect those of the United States Government or any agency thereof. Reference herein to any social initiative (including but not limited to Diversity, Equity, and Inclusion (DEI); Community Benefits Plans (CBP); Justice 40; etc.) is made by the Author independent of any current requirement by the United States Government and does not constitute or imply endorsement, recommendation, or support by the United States Government or any agency thereof.

ANL/CFCT-25/9

Assessment of Active Metal Removal from Pyroprocessing Salt by Electrodeposition

Chemical and Fuel Cycle Technologies Division

About Argonne National Laboratory

Argonne is a U.S. Department of Energy laboratory managed by UChicago Argonne, LLC under contract DE-AC02-06CH11357. The Laboratory's main facility is outside Chicago, at 9700 South Cass Avenue, Argonne, Illinois 60439. For information about Argonne and its pioneering science and technology programs, see www.anl.gov.

ANL/CFCT-25/9

Assessment of Active Metal Removal from Pyroprocessing Salt by Electrodeposition

by
L. Gardner, T. Lichtenstein and M.A. Rose
Chemical and Fuel Cycle Technologies Division, Argonne National Laboratory

June 30, 2025

CONTENTS

FIGURES

FIGURES (cont.)

TABLES

ACKNOWLEDGEMENTS

This report was produced under the auspices of the US DOE NE-43 Material Recovery and Waste Form Development Campaign. Issuance of this report meets milestone M3FT-25AN0301020110. The authors gratefully acknowledge efforts by Dr. Jarrod Gesualdi and Dr. Yifeng Liao for microscopy of samples. Compositional analyses of samples provided by Ms. Kristin DeAngeles, Ms. Susan Lopykinski, Dr. Seema Naik, and Ms. Yifen Tsai (Argonne Analytical Chemistry Laboratory) are gratefully acknowledged. This work was conducted at Argonne National Laboratory and supported by the U.S. Department of Energy, Office of Nuclear Energy, under Contract DE-AC02-06CH11357.

1. INTRODUCTION

Active metals present in used nuclear fuel dissolve into the salt during pyroprocessing, but are not recovered during electrorefining or drawdown operations due to their chemical stability in the salt. The accumulation of ^{137}Cs and ^{90}Sr in process salt over time increases the heat load and ionizing radiation level of the salt such that it must be replaced frequently, resulting in a significant amount of salt waste. An effective means of removing active metals from the molten salt to enable recycle of the electrolyte (e.g., LiCl/KCl) would increase the efficiency of pyroprocessing and decrease the volume of salt waste requiring disposal.

A previous report summarized issues to be addressed when developing a removal strategy and assessed existing methods and technological gaps to their application (Rose and Thomas 2023). Active metals are extremely stable in molten salt as chlorides—even more stable than the LiCl-KCl eutectic base salt used for pyroprocessing fuel—which makes removing them a challenge. Sufficiently strong atomic interactions occur between active metal species and reactive metals (e.g. Bi, Sb, Cu, Al) that make the electrodeposition of active metal fission products into reactive liquid metal electrodes thermodynamically favorable (Nigl et al., 2020) such that removal of cesium and strontium by electrodeposition may be feasible. In this process, active metal species in the salt are reduced to metals at the surface of the liquid metal electrode by an electrochemically-driven reaction and then diffuse into the bulk of the liquid metal electrode. Figure 1 depicts the processes occurring during active metal drawdown. Nigl et al. (2020) deposited barium and strontium from LiCl-KCl-($BaCl_2$,$SrCl_2$) salts into different active metals including Bi, Sb and Bi-Sb alloys.

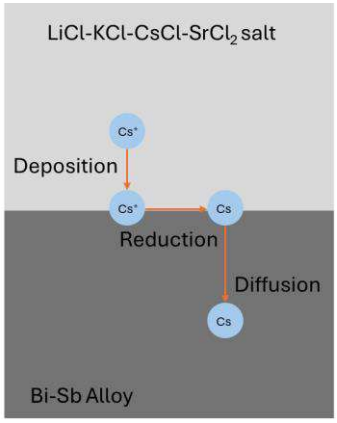

Figure 1. Schematic of processes occurring during deposition and incorporation of active metals at the salt-metal interface.

Work summarized in this report extended that to include cesium-bearing salts. The feasibility of recovering cesium from LiCl-KCl pyroprocessing salt through electrodeposition into liquid metals was initially assessed in 2024 by performing tests electrodepositing cesium from a LiCl/KCl salt into liquid bismuth and 50-50 mol% Bi-Sb alloy electrodes (Lichtenstein et al. 2024). In Figure 2, the reduction potentials (E^0_A) for pure lithium, potassium, strontium and cesium are compared to

the equilibrium potentials for depositing the individual species into liquid bismuth (E^{eq}_A) at concentrations of 5 mol % (open squares) and 10 mol % (filled squares) of each alkali metal in the alloy. Note that due to a lack of availability of measurements for Cs^+ reduction in bismuth, the electromotive force value measured for Rb^+ in bismuth (Petric, 1988) is plotted to represent the reduction potential of Cs^+ in bismuth and labeled as Cs^+/Cs-Bi in Figure 2. Based on this thermochemical data, electrodeposition of active metals into liquid antimony and the liquid Bi-Sb alloy was conducted at a constant voltage of 0.1 V vs. Li^+/Li^0 (indicated as Deposition Potential in Figure 2). This voltage provides the largest driving force for deposition without promoting the generation of lithium metal in the salt by remaining 100 mV below the standard potential for lithium reduction.

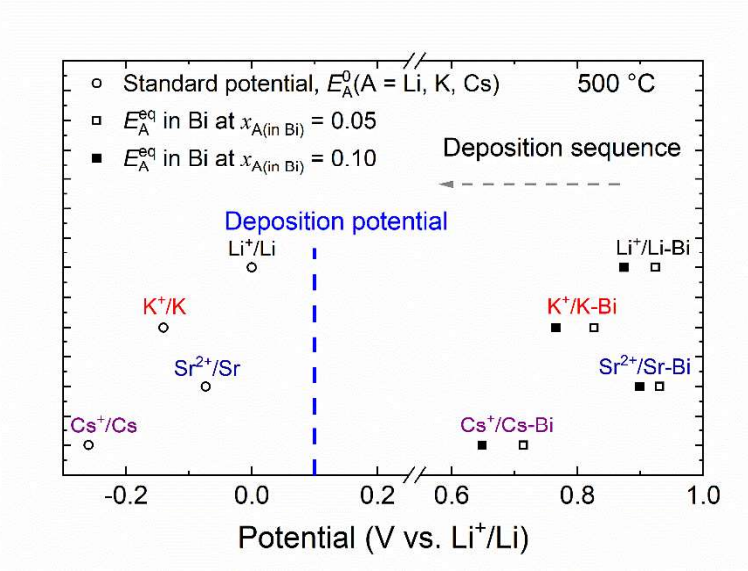

Figure 2. Equilibrium potentials for active metals at 5 and 10 mol % in bismuth at 500 °C

Based on Figure 2, co-deposition of lithium with cesium from a LiCl-KCl-CsCl salt into liquid metal electrodes is expected and was observed in tests in 2024 (Lichtenstein et al., 2024). In those tests, cesium was found to accumulate preferentially in the antimony-rich phases of the solidified Bi-Sb alloy. Some tests were performed using an aluminum mesh lithium depletion electrode to locally deplete lithium from salt of in the vicinity of the liquid metal electrode to increase cesium recovery. Lithium alloys with this electrode material without generating pure lithium metal, thereby depleting lithium from salt near the liquid metal electrode surface to decrease the amount of lithium co-deposited into the liquid metal.

The work summarized herein was done to establish the effectiveness of electrodeposition for recovering active metals at liquid metal cathodes by optimizing the use of a lithium depletion electrode and assess deposition of active metals into a pure antimony electrode.

2. Methods

Separate mixtures of LiCl (ACS Reagent, 99.9 %), KCl (ACS Reagent, 99.9%), $SrCl_2$ (anhydrous 99.99%) and CsCl (anhydrous, 99.9%) were used for each test and each reagent was baked out overnight (approximately 16 hours) at 300 °C to remove adsorbed water before use. Appropriate masses of each salt were added to an alumina crucible to generate approximately 100 g of salt for each test comprised of 90 wt % 58 LiCl - 42 KCl mol % eutectic with 7 wt % CsCl and 3 wt% $SrCl_2$ (2.5 at % Cs, 1.1 at % Sr), with the exception of the first test, Cs-Bi/Sb-0 with parallel deposition to the lithium depletion and liquid metal electrodes, which contained 10 wt % CsCl and excluded $SrCl_2$. Working electrodes consisted of either antimony or an alloy of equimolar amounts of bismuth and antimony that were contained in boron nitride crucibles. Tests using a bismuth-antimony alloy electrode were conducted at 500 °C and tests using an antimony liquid metal electrode were conducted at 650 °C. An electrode made with 65 mol % lithium 35 mol % bismuth alloy contained in a boron nitride crucible with LiCl-KCl overtop and a tungsten rod shielded from the electrolyte by a stainless steel tube was used as the reference electrode. The open circuit potential of this alloy is known to be 0.716 V vs. Li^+/Li^0 at 500 °C (Gąsior and Moser, 2001). Tungsten rods served as the electrical leads for the working and reference electrodes. A graphite rod attached to an 18-8 stainless steel rod served as the counter electrode in all tests.

A schematic of the electrochemical cell configuration is shown in Figure 3a and a circuit diagram of the cell is shown in Figure 3b. The lithium depletion electrode mesh was placed around the working electrode containing the liquid metal, as depicted in Figure 3a. Separate circuits connected the anode to the lithium depletion cathode and the liquid metal cathode, as can be seen in Figure 3b. The boron nitride crucible (white in Figure 3b) containing the liquid metal electrode also electrically isolated it from the lithium depletion electrode. The cathodic current measured for each electrode indicates the reductive deposition and co-deposition processes occurring and the charge indicates the cumulative extent.

Deposition tests in the bismuth-antimony alloy liquid metal electrode used a lithium depletion electrode constructed of 6061 aluminum alloy and operated at 500 °C. Pure antimony has a melting point of 631 °C therefore deposition tests into pure antimony electrodes were conducted at 650 °C. Aluminum has a melting point of 663 °C. It was therefore likely that an aluminum mesh constructed lithium depletion electrode would soften at the test temperature of 650 °C for deposition tests into antimony. Therefore, lithium depletion electrodes were constructed of brass (m.p. > 900 °C) for deposition tests into pure antimony. In all tests, the electrochemical cell was heated for 18 hours prior to imposing a voltage.

The depletion electrode and liquid metal electrode were removed from the salt at the conclusion of a deposition test to prevent back reaction of deposited active metals with salt.

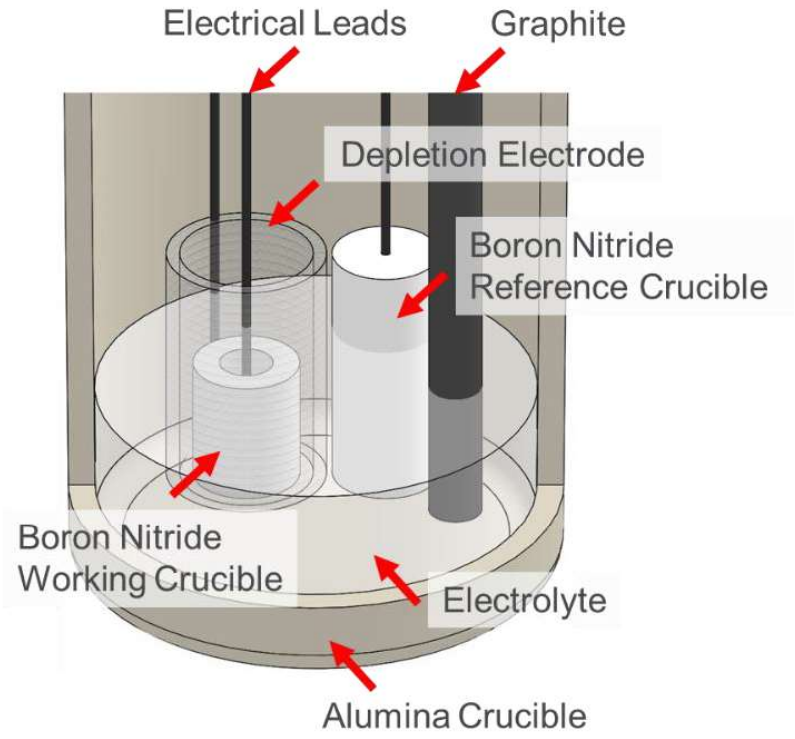

(a)

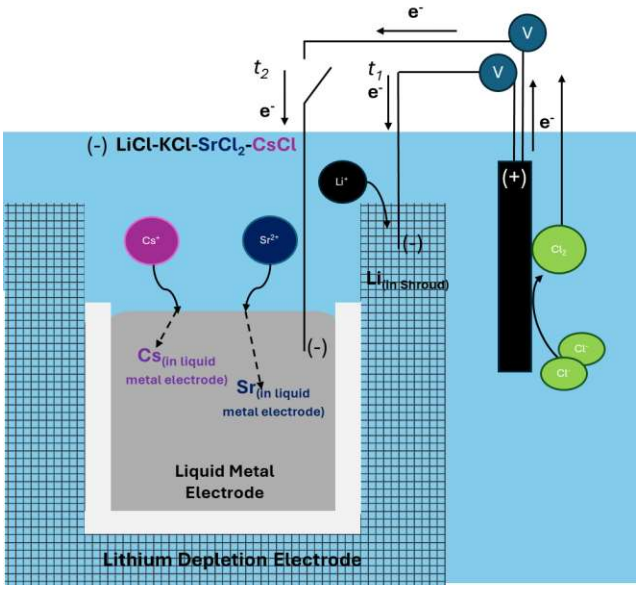

(b)

Figure 3. Schematic (a) and circuit diagram (b) of the electrochemical cell used to deposit active metals into liquid metals.

Tests were conducted after passing 0, 50, or 100 coulombs of charge to the depletion electrode prior before polarizing the liquid metal electrode to determine the sensitivity of active metal removal to the amount of charge to the lithium deposition electrode prior to enhance active metal removal. Test parameters are summarized in Table 1.

Table 1. Test parameters for active metal drawdown tests.

Test ID	Salt Composition, wt %	Liquid Metal Cathode Material, wt %	Operating Temperature, °C	Charge to depletion electrode prior to deposition into liquid metal, coulombs	Depletion Electrode Material
Cs-Bi/Sb-0	40 LiCl–50 KCl–10 CsCl	50 Bi – 50 Sb	500	0	Aluminum
Cs/Sr-Bi/Sb-50	40 LiCl–50 KCl–7 CsCl–3 $SrCl_2$	50 Bi – 50 Sb	500	50	Aluminum
Cs/Sr-Bi/Sb-100	40 LiCl–50 KCl–7 CsCl–3 $SrCl_2$	50 Bi – 50 Sb	500	100	Aluminum
Cs/Sr-Sb-1	40 LiCl–50 KCl–7 CsCl–3 $SrCl_2$	100 Sb	650	100	Brass
Cs/Sr-Sb-2	40 LiCl–50 KCl–7 CsCl–3 $SrCl_2$	100 Sb	650	100	Brass

Characterization of the liquid metal electrodes after deposition testing was done by using scanning electron microscopy with associated energy-dispersive X-ray spectroscopy (SEM/EDS) to detect the distributions of cesium and strontium. The entire electrode from each test was embedded in epoxy, sectioned vertically perpendicular to the salt metal interface and dry-polished to 1200 grit in an inert atmosphere glovebox prior to characterization. The electrode from Cs/Sr-Sb-1 was not characterized but is retained for future characterizations. It is expected that the deposited elements dissolved into the liquid metal and became distributed in the near-surface region during the test due to diffusion and possibly convection. When the electrode is removed and cooled, the elements may be preferentially sequestered in particular phases or regions as the electrode solidifies.

Figure 4 depicts a cross sectioned electrode in the boron nitride crucible prepared for SEM analysis with a red box indicating a typical analysis region. Analyses were performed to gain insights into the distribution of active metals in the alloys and salt near the salt-metal interface. Alloy material in the second half of sectioned products from the Cs/Sr-Bi/Sb-50 and Cs/Sr-Bi/Sb-100 tests were removed from the epoxy, dissolved in nitric acid and then analyzed by using inductively coupled plasma- mass spectroscopy (ICP-MS) for bulk composition. Samples of salt were taken before and after the Cs/Sr-Bi/Sb-50 and Cs/Sr-Bi/Sb-100 tests by collecting a sample of cooled solidified salt. These samples were then dissolved in nitric acid and the elemental concentrations of lithium, potassium, cesium and strontium in the solutions were measured by using ICP-MS. The difference in the results of these analyses provides a measure of the amounts of cesium and strontium that were removed from the salt.

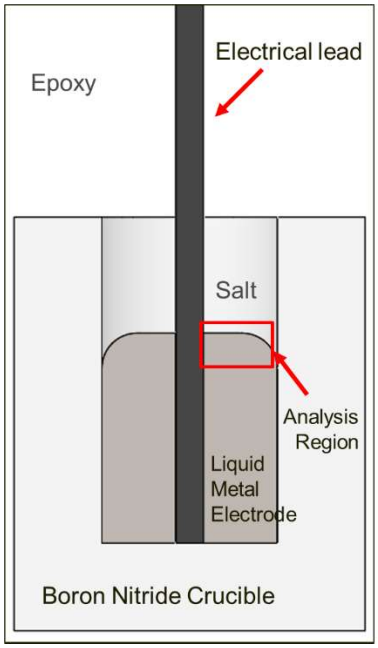

Figure 4: Schematic of a typical sectioned electrode prepared for SEM analysis.

3. DEMONSTRATIONS OF ACTIVE METAL DEPOSITION INTO LIQUID METALS

3.1 Deposition Tests into 50Bi-50Sb Alloy at 500°C

3.1.1 Cs-Bi/Sb-0

In the Cs-Bi/Sb-0 test, the depletion electrode and liquid metal (50Bi-50Sb) alloy electrode were polarized at 0.1 V vs. Li^+/Li^0 simultaneously. Lithium depletion was conducted simultaneously with active metal deposition in this test to provide a baseline for comparison for later tests with 50 or 100 coulombs of lithium depletion performed prior to active metal deposition. Figure 5 shows the chronocoulometric data for this test including the measured current vs time and the calculated charge passed vs time at each electrode. Over the length of the test, the depletion electrode collected a total of ~450 coulombs of charge at ~300 mA. This corresponds to the deposition of lithium into the aluminum electrode.

The initial current through the liquid metal electrode was 20 mA but the current slowly decreased over the duration of the test (2000 s). Current is expected to be much higher at the lithium depletion electrode than at the liquid metal electrode because the lithium depletion electrode has a much higher surface area, being constructed of a mesh; the surface area of the lithium depletion electrode

was not estimated. The area of the liquid metal electrode is confined to the circular surface of the pool of liquid metal, which corresponds to the inner diameter of the crucible.

After nearly 20,000 s (5.6 h) the current at the liquid metal electrode became unstable and negligible additional charge was passed. At this point the test was stopped. The total charge passed to the liquid metal electrode over the duration of the test was ~170 coulombs. The electrodes were removed from the salt immediately after polarization was stopped to prevent possible back-reactions with lithium in the salt.

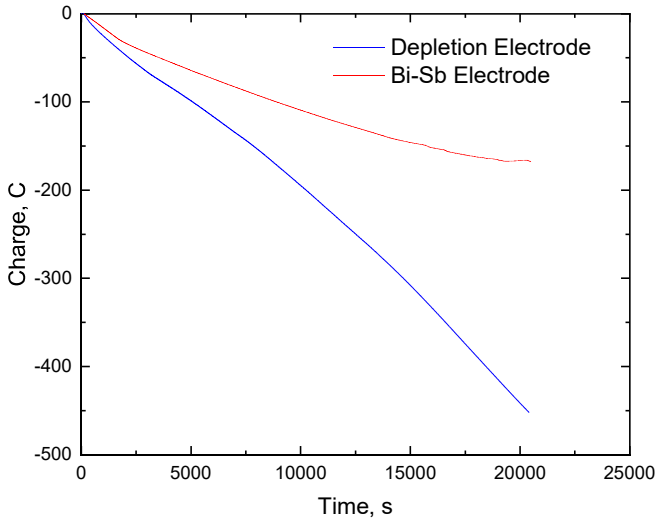

(a)

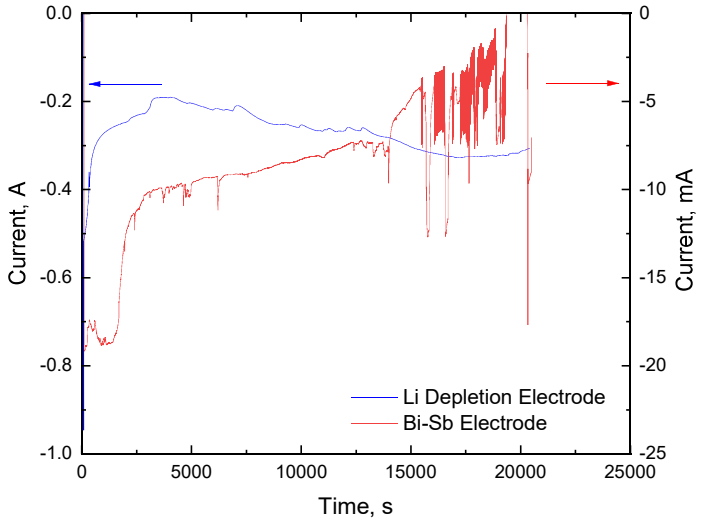

(b)

Figure 5. Chronocoulometric measurements during test Cs-Bi/Sb-0 with parallel deposition to the lithium depletion and 50Bi-50Sb alloy electrode with rapid removal of the electrode after deposition (a) charge and (b) current.

3.1.2 Cs/Sr-Bi/Sb-50

In the Cs/Sr-Bi/Sb-50 test, the depletion electrode was polarized to 0.1 V vs. Li^+/Li^0 for ~ 6000 s so that 50 coulombs of charge had been passed before the liquid metal electrode was polarized. Figure 6 shows the chronocoulometric data for the test including the measured current vs time and the calculated charge passed vs time at each electrode. A vertical dashed line in Figure 6 indicates the time the liquid metal electrode was polarized and a horizontal dashed line in Figure 6a indicates the charge at the depletion electrode when the liquid metal electrode was polarized. When the liquid metal electrode was first polarized, the current at the depletion electrode became net anodic for approximately 20 minutes before returning to a low cathodic value. This spike in anodic current at the depletion electrode can have several causes: the electrical leads to the active metal deposition electrode and the depletion electrode may have been in contact, the depletion electrode and anode may have been in contact, or the anode was inappropriately sized to have two electrolyzers running at the same time. The very low cathodic currents at the large surface area depletion electrode after 20 minutes of anodic current indicate that a short circuit may have existed. Modifications to the anode design may also be considered which increase the size of the electrode to allow for the use of two electrolyzers or the use of two separate anodes.

When the liquid metal electrode was polarized, a cathodic current of ~100 mA was induced at the liquid metal electrode. This current changed rapidly to a value of ~25 mA over the first ~ 1200 s and then decreased to near zero after about 6000 s of deposition until ~120 coulombs had been passed. At 6000 s into active metal deposition (12000 s total test duration) the current changed from net cathodic to 20 mA net anodic by the time the test was stopped. This reverse in the current at the liquid metal electrode during deposition indicates that the dominant process at the electrode surface is no longer deposition of active metals. The magnitude of the current at the depletion electrode appears equal and opposite to the current at the liquid metal. This is further evidence that a short circuit occurred (e.g., depletion electrode to anode) when the liquid metal electrode was polarized.

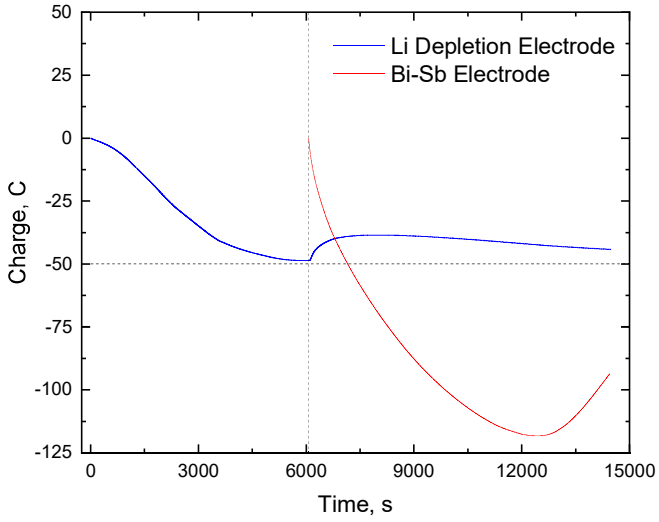

(a)

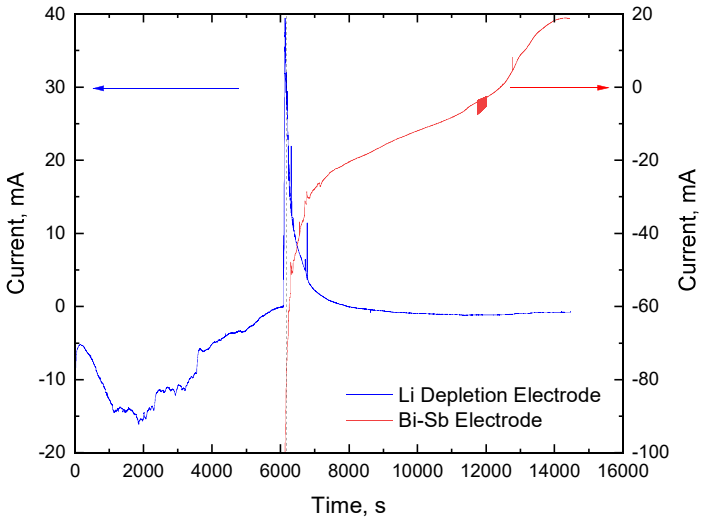

(b)

Figure 6. Chronocoulometric measurements during test Cs/Sr-Bi/Sb-50 where 50 coulombs was passed to the lithium depletion electrode prior to deposition into 50Bi-50Sb alloy electrode with rapid removal of the electrode after deposition.

3.1.3 Cs/Sr-Bi/Sb-100

In the Cs/Sr-Bi/Sb-100 test, the lithium depletion electrode was polarized to 0.1 V vs. Li^+/Li^0 for ~6000 s to pass 100 coulombs of charge prior to polarizing the liquid metal electrode. Figure 7 shows the chronocoulometric data for the test including the measured current vs time and the calculated charge passed vs time at each electrode. Current at the depletion electrode during the first 1500 s was unstable and dropped from nearly 100 mA to < 25 mA. After ~80 coulombs passed, the current dropped to <5 mA and remained steady at this level for the remainder of the test. Vertical dashed lines in Figure 7 indicate the time that the liquid metal electrode was first polarized and the horizontal dashed line in Figure 7a indicates the charge passed to the depletion electrode at the time the liquid metal electrode was polarized. Polarizing the Bi-Sb alloy did not measurably perturb the depletion electrode current during this test as it had in the Cs/Sr-Bi/Sb-50 test.

The current at the liquid metal electrode was intially steady at ~10 mA, but after 3000 s drifted toward zero. The test was stopped when the current became anodic after ~10,000 s of deposition at the liquid metal electrode. The total charge passed was ~30 coulombs, which is significantly less than in previous tests. The depletion electrode construction failed during retrieval from the salt and the electrodes were not removed immediately after the test. Back reaction of the product is expected to have occurred. The low currents and charge passed to the liquid metal electrode along with the mechanical failure upon withdrawl from the salt may indicate there was insufficient electrical conductivity to the liquid metal electrode during this test.

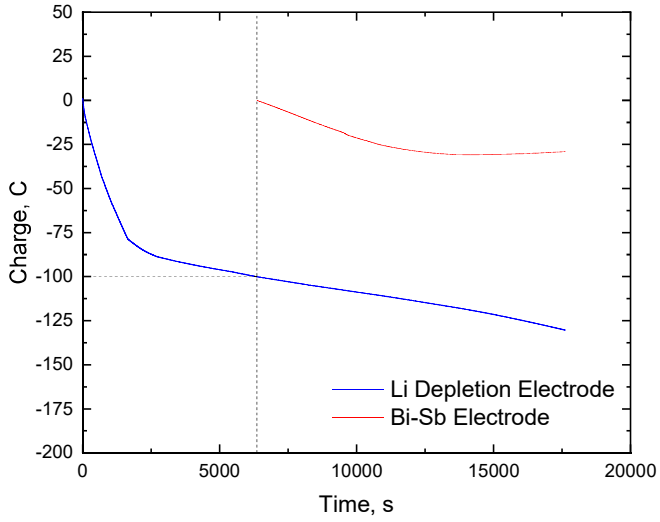

(a)

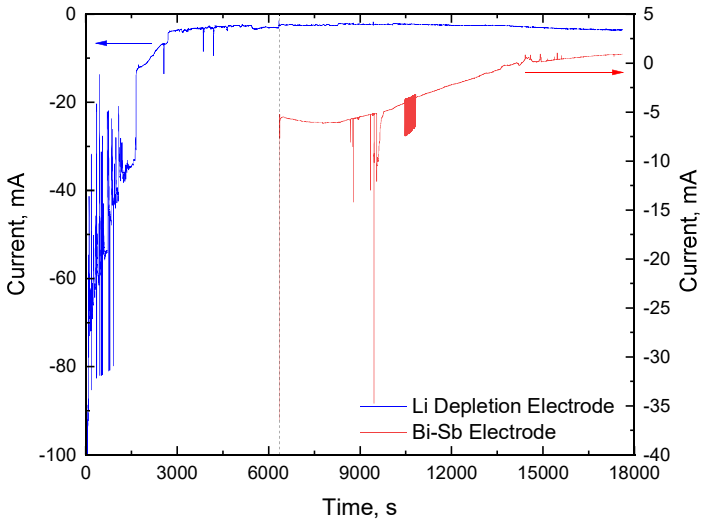

(b)

Figure 7. Chronocoulometric measurements during test Cs/Sr-Bi/Sb-100 where 100 coulombs was passed to the lithium depletion electrode prior to deposition into 50Bi-50Sb alloy electrode and the electrode cooled in the salt after deposition.

3.2 Deposition Tests into an Antimony Electrode at 650°C

3.2.1 Cs/Sr-Sb-1

In the Cs/Sr-Sb-1 test, 100 coulombs of charge were passed to the lithium depletion electrode in 127 s prior to polarization of the antimony electrode to 0.1 V vs. Li^+/Li^0. Figure 8 shows the chronocoulometric data for this test, with the inset highlighting the first 500 s of the test. The vertical dashed line in the inset indicates the time the liquid metal electrode was polarized. The 800 mA current measured at the brass depletion electrode was considerably higher than that achieved in the tests with depletion electrodes made of aluminum that were discussed in Section 3.1. This may be due to the greater weldability of brass compared to aluminum and better electrical connection between the lead wire and the depletion electrode material. A total of 7000 coulombs of charge were passed to the lithium depletion electrode over the duration of the deposition.

At 127 s the deposition at the antimony electrode at 0.1 V vs. Li^+/Li^0 was begun. The current through the antimony electrode was extremely low at < 2 mA, but remained cathodic over the duration of the test, ~8000 s. A total of ~15 coulombs of charge was passed through the antimony electrode. The brass depletion electrode fabricated for this test was not strong enough to support the weight of the liquid metal electrode during removal at 650 °C, and the electrode was not retrieved. This caused the liquid metal electrode to cool in the salt, and it was not analyzed.

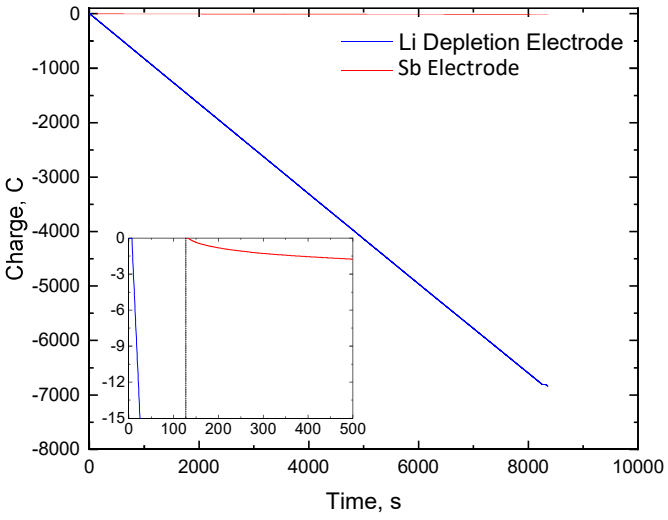

(a)

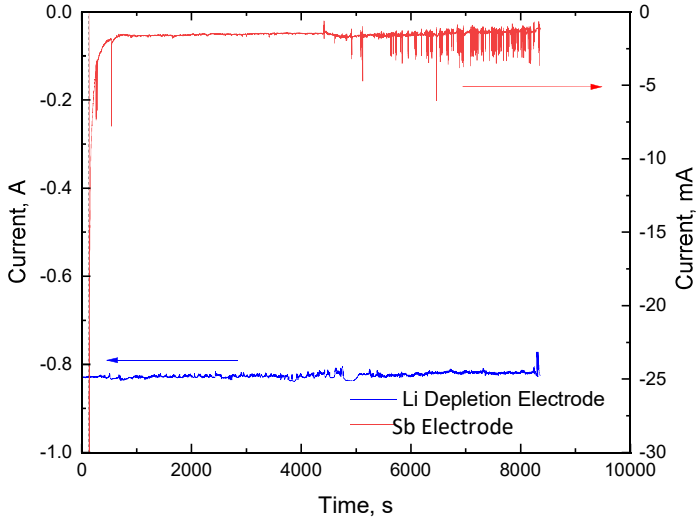

(b)

Figure 8. Chronocoulometric measurements during Test Cs/Sr-Sb-1 where 100 couolombs were passed to the lithium depletion electrode prior to deposition into the antimony electrode but the electrode was not able to be removed promptly after the test.

3.2.2 Cs/Sr-Sb-2

In the Cs/Sr-Sb-2 test, 100 coulombs were passed to a newly constructed brass lithium depletion electrode prior to starting deposition at the antimony electrode. Chronocoulometric data for the test is shown in Figure 9, where the vertical dashed lines indicate the time the liquid metal electrode was polarized. Current at the depletion electrode was initially > 250 mA and decreased to near zero over the duration of the test.

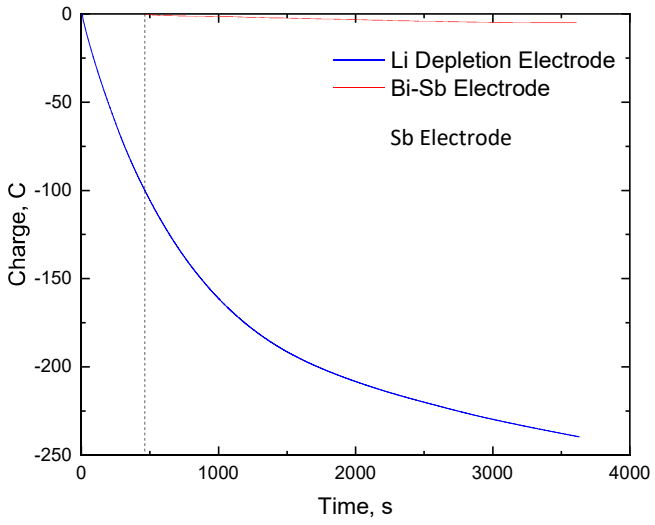

(a)

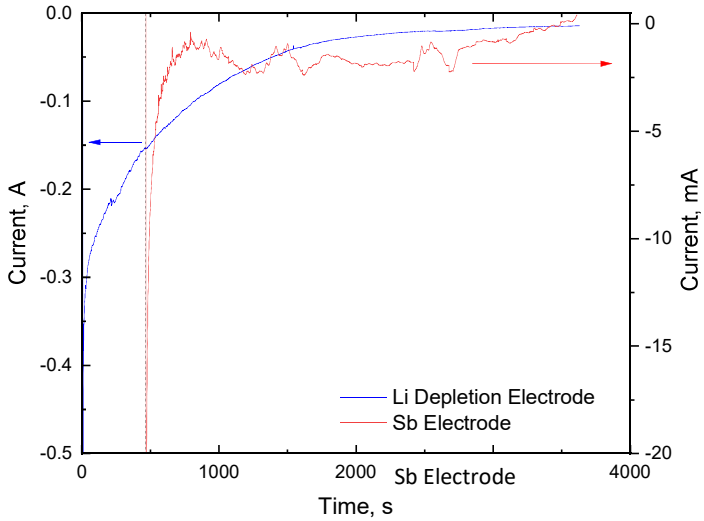

(b)

Figure 9. Chronocoulometric measurements during Test Cs/Sr-Sb-2 where 100 coulombs were passed to the lithium depletion electrode prior to deposition into the antimony electrode and the electrode was removed promptly after deposition.

At ~500 s, the antimony electrode was polarized to 0.1 V vs. Li^+/Li^0 for active metal deposition and current began at >10 mA and decreased to < 2.5 mA over the duration of the test. A total of only ~5 coulombs of charge were passed to the antimony electrode.

After the deposition test was terminated, the electrodes were withdrawn from the salt to cool to prevent back reaction of any deposited active metals with lithium or potassium in the salt. Figure 10 shows photographs of this brass constructed lithium depletion electrode before and after use.

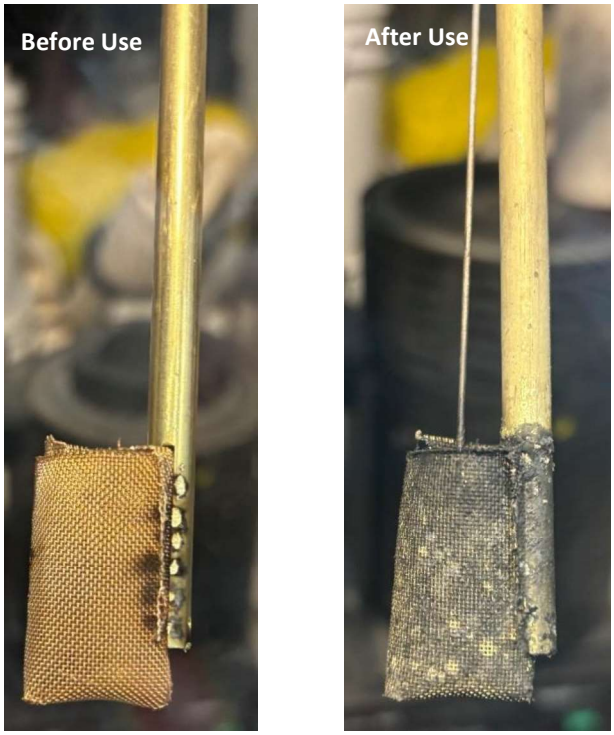

Figure 10. Photographs of the lithium depletion electrode constructed of brass before and after deposition test Cs/Sr-Sb-2

The distinct color change of both the mesh and rod indicates successful lithium deposition. In the after-use photograph, the thinner lead wire is submerged in the antimony electrode, which is inside the brass mesh basket.

4. ANALYSES OF ELECTRODES

Alloy electrodes from some tests were embedded in epoxy and cross sectioned vertically perpendicular to the salt-alloy interface. Epoxy was used to maintain the salt/metal interfaces and electrode geometry during cutting and polishing. One cross-sectioned surface was dry-polished in an argon atmosphere glovebox. The sectioned and polished electrodes were transported from the glovebox to the SEM inside a container under argon atmosphere. It is expected that these samples contained deposited lithium metal and were highly reactive to moisture in the air. The samples were briefly exposed to air during transfer from the container to the SEM chamber, which was quickly evacuated. Methods to mitigate the effects of air exposure are being evaluated. SEM/EDS analysis was performed to examine the distribution of active metals near the surface of the metal electrode that was in contact with the salt when the electrode was removed from the salt and cooled. Secondary electron imaging (SEI) was used to evaluate texture and back-scattered electron imaging (BSE) was used to highlight compositional differences: heavier elements appear brighter than lighter elements. Although EDS does not detect lithium, the brightness of phases in SEM-BSE images is sensitive to its presence. Compositional EDS analyses were performed as spot analyses, small area analyses, and to generate X-ray maps of the imaged region. Analyses of the solidified electrode surfaces are more sensitive to deposited alkali metal than analysis of concentration changes in the depleted bulk salt.

A piece of the as-prepared Bi-Sb alloy was mounted in epoxy and polished for SEM analysis for comparison with electrodes from deposition tests. Figure 11 shows an SEM-BSE photomicrograph of the as-prepared Bi-Sb alloy. There are darker regions rich in antimony in the more abundant lighter regions rich in bismuth throughout the alloy.

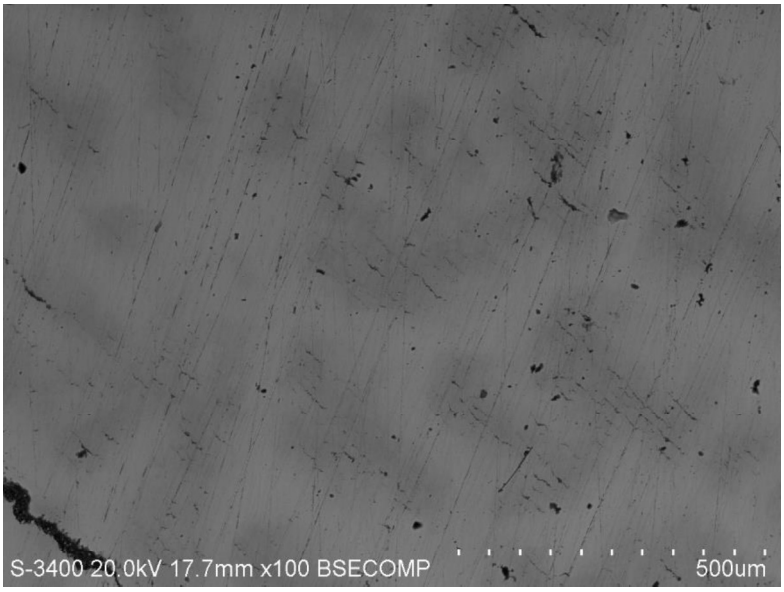

Figure 11. SEM-BSE photomicrograph of the as-prepared 50Bi-50Sb alloy

Figure 12 shows the phase diagram for the bismuth antimony alloy with a vertical red dashed line at the 50 Bi -50 Sb mol % (37 Bi -63 Sb at. %) composition used in the active metal deposition electrodes in these tests (Okamoto, 2012). An incongruently melted phase exists at 500 °C into which the active metal deposition occurred during tests presented in this report, consisting of antimony-rich solid phases in a bismuth-rich liquid.

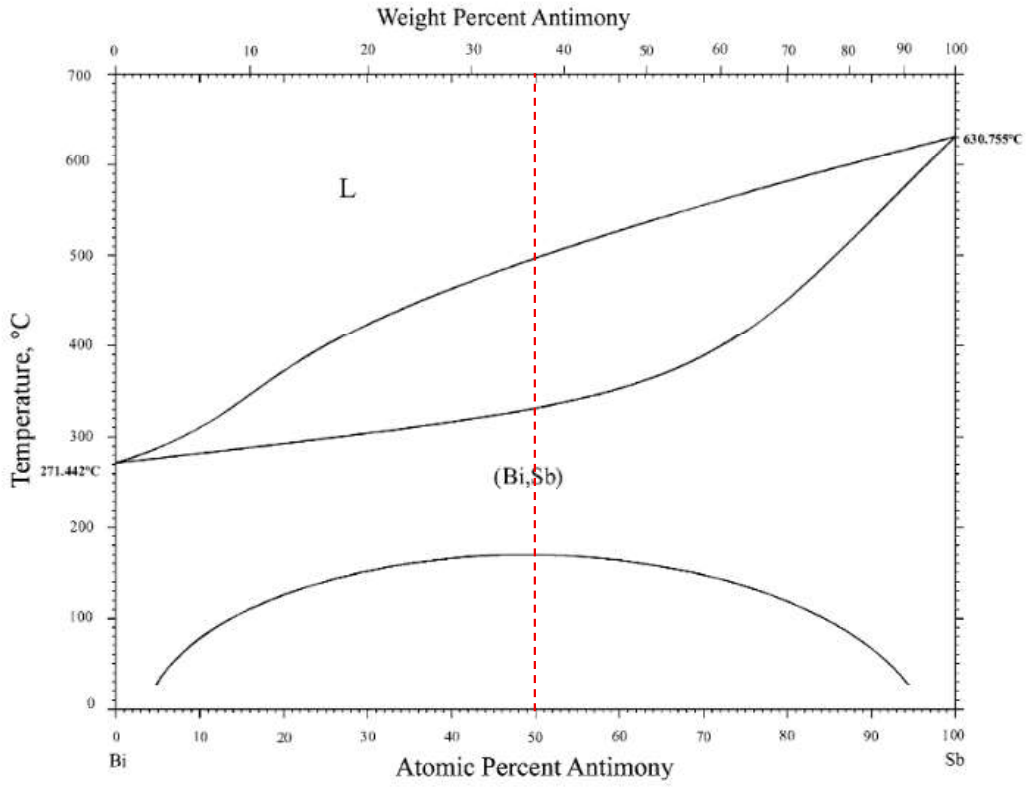

Figure 12. Phase diagram of bismuth antimony alloy from Okamoto, 2012.

EDS point analyses (Figure 13 and Table 2) were conducted to gauge senstivity of the EDS analyses to the presence of Cl, K, Cs and Sr in the alloy and to gain insight into the microstructures seen in analyses of liquid metal electrodes.

In Figure 13, identified locations in both the lighter (1-8) and darker (9-14) grey regions were analysed by EDS spot analyses. Table 2 lists the normalized concentrations of bismuth, and antimony as well as representative background responses for chlorine, potassium, cesium and strontium for comparison with analyses of test electrodes.

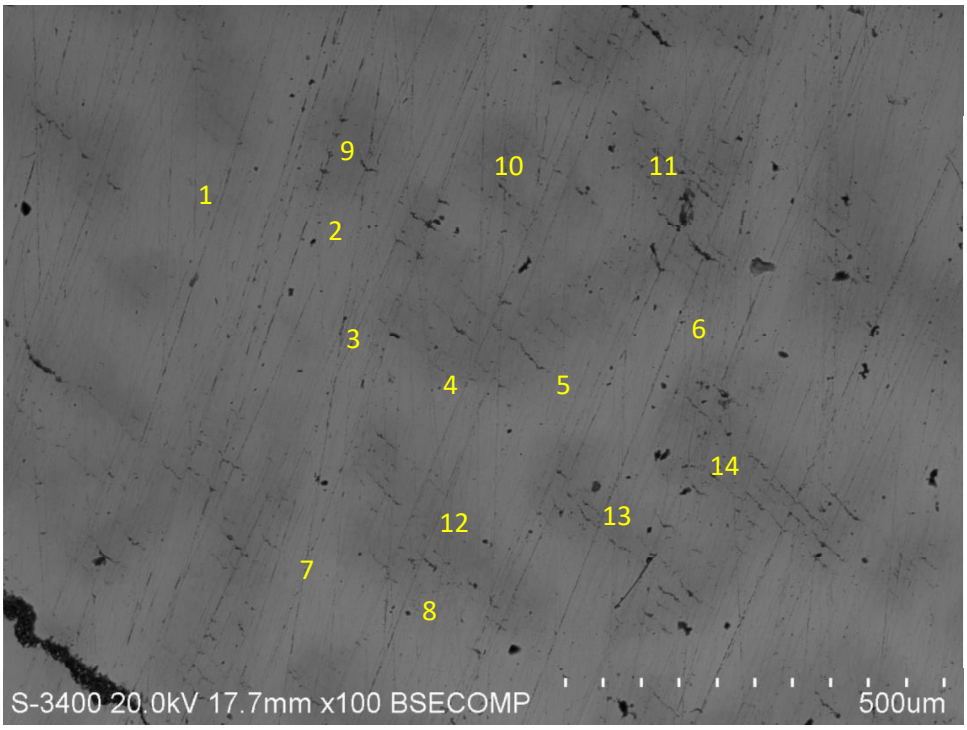

Figure 13. SEM-BSE photomicrograph from Figure 10 with marked locations for EDS analysis.

In Table 2, locations 1-8 have > 68 at. % bismuth while regions 9-14 have > 62 at. % antimony, confirming the expectation that distinct bismuth-rich and antimony-rich phases form in the 50 Bi-50 Sb mol % alloy upon cooling. This is expected from the phase diagram in Figure 12. Cesium is not detected in any of the locations in Figure 13, while EDS detects low apparent concentrations of strontium (up to 1.3 at. %), chlorine (up to 6.6 at. %), and potassium (up to 0.3 at %), particularly in bismuth-rich locations 1-8. Note that there is chlorine in the epoxy, which may have contaminated the surface during polishing. These are used as background levels for analyses of electrodes from deposition tests.

Table 2. Normalized concentrations of elements (at. %) in the as-prepared Bi-Sb alloy, determined by EDS analysis at locations indicated in Figure 13.

Concentration in atom %						
Point Number	Antimony	Bismuth	Cesium	Strontium	Chlorine	Potassium
1	24.5	70.3	0	0.9	4.3	0
2	15.0	79.4	0	0.7	4.6	0.3
3	12.7	79.6	0	1.3	6.4	0
4	22.0	72.5	0	1.2	4.3	0
5	25.8	68.0	0	0.6	5.5	0.2
6	17.3	76.9	0	1.2	4.6	0
7	12.8	81.5	0	1.0	4.7	0
8	19.6	72.6	0	1.3	6.6	0
9	80.3	19.1	0	0	0.6	0
10	62.1	35.1	0	0.7	2.1	0
11	84.0	14.5	0	0.5	0.8	0.2
12	79.7	20.3	0	0	0	0
13	69.7	26.3	0	0.4	3.7	0
14	68.0	29.1	0	0.1	2.8	0

4.1 Analyses of Electrodes from Deposition Tests into 50Bi-50Sb Alloy Electrodes

4.1.1 Cs/Sr-Sb-0

The metallic alloy generated during deposition of cesium into a Bi-Sb alloy at 500 °C during test Cs/Sr-Sb-0 is shown in Figure 14. In this test, the lithium depletion electrode and active metal electrode were polarized simultaneously and a total of 170 coulombs of charge were passed through this alloy electrode, indicating deposition occurred. This test represents the baseline for comparison of subsequent tests at 50 and 100 coulombs of lithium depletion pior to active metal deposition.

Figure 14a is a BSE photomicrograph of the epoxy-mounted cross sectioned alloy electrode, which was removed from the boron nitride crucible prior to encapsulation in epoxy. The salt layer at the top of the electrode broke off the electrode prior to encapsulation. The flat surface at the bottom of the image in Figure 14a is the bottom of the electrode which was in contact with the bottom of the crucible during the test and the rounded top edge of the alloy at the top of the image in Figure

14a was the salt-alloy interface. A magnified BSE photomicrograph of the top surface of the alloy outlined in red in Figure 14a is shown in 14b. The dark band at the top of the high magnification image is epoxy and the bright region above that is an artifact of charging during SEM analysis.

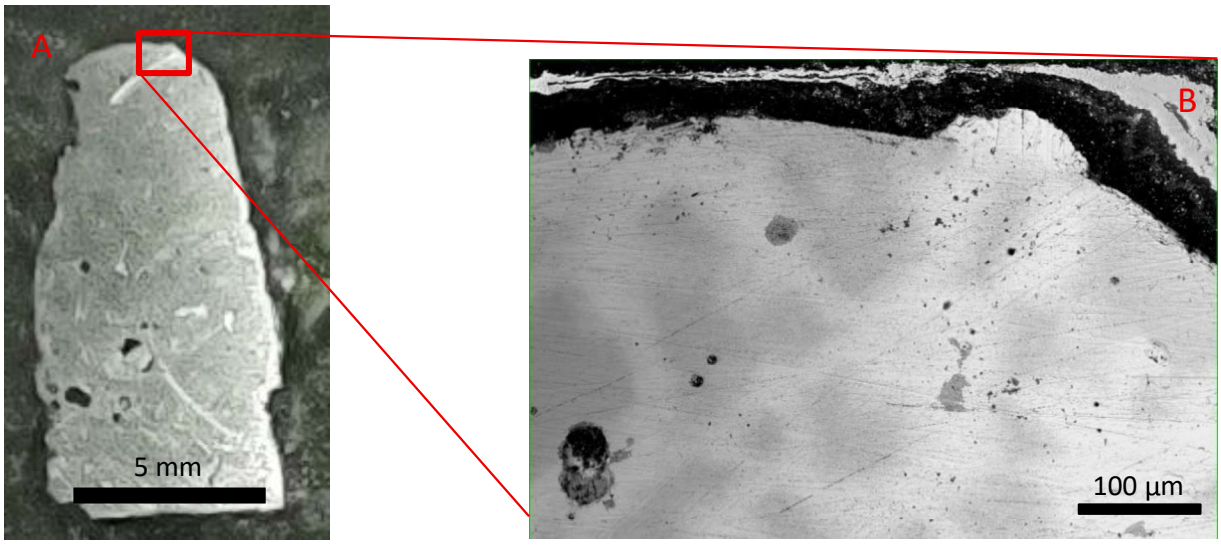

Figure 14. SEM-BSE photomicrographs of the Bi-Sb alloy electrode from the Cs-Bi/Sb-0 deposition test (a) low magnification and (b) high magnification.

In Figure 14b, the dark grey regions correspond to the antimony-rich phases and the light grey to the bismuth-rich phases similar to the microstructure seen in analyses of the as-prepared alloy in Figure 11. Figure 16 show EDS X-ray maps of the region in Figure 14b for bismuth, antimony, cesium, and potassium. The distribution of bismuth-enriched and anitmony-enriched regions is confirmed by the EDS X-ray maps showing distinct regions of antimony and bismuth in blue and yellow, respectively, in Figure 16. This same microstructure was observed in Bi-Sb alloys used in previous work (Lichtenstein et al. 2024). Strontium was not present in the salt used in this test and therefore it was not analyzed for. Lithium is not detected by EDS.

The map for cesium in Figure 15 is correlated with the map for antimony and indicates a slight preference for the antimony-rich phase, most notable in the antimony-rich region at the upper right-hand side of the image near the electrode surface. Potassium was detected and is expected to have co-deposit with cesium. A uniform detection of potassium covers the field of view of the alloy, but not in the epoxy layer. This is similar to the analysis of the as-prepared alloy and may be background signal.

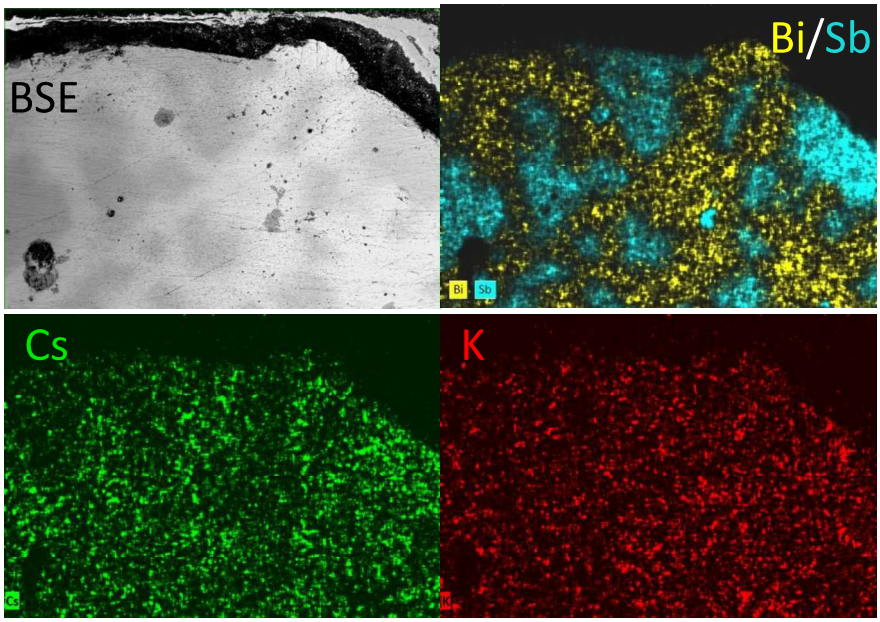

Figure 15. EDS X-ray maps of the region imaged in Figure 14b, the Bi-Sb alloy electrode from parallel deposition test (Cs-Bi/Sb-0) analyzed for the presence of Bi, Sb, Cs, and K.

Figure 16 indicates locations on the region of the alloy imaged in Figure 14b identified for EDS point analysis. Locations 1-4 are in dark grey antimony-rich regions, Locations 5 and 6 are in darker grey inclusions, and Locations 7-10 are in light grey bismuth-rich regions.

Table 3 shows the measured concentrations of bismuth, antimony, and cesium. Locations 1-4 are > 69.9 at. % antimony with no detectable cesium or potassium. Locations 5 and 6 are inclusions of pure antimony and locations 7-10 are > 57 at. % bismuth with no detectable cesium or strontium.

Most notable about these spot analyses is that cesium is not detected at any location, which is contrary to the X-ray map. The difference can be attributed to the physical difference in the measurement techniques: the X-ray maps are generated as the electron beam is repeatedly rasterering across the entire field of view, whereas spot analyses are made with the beam fixed on one location. Localized charging may cause elements to migrate out of the analyzed volume.

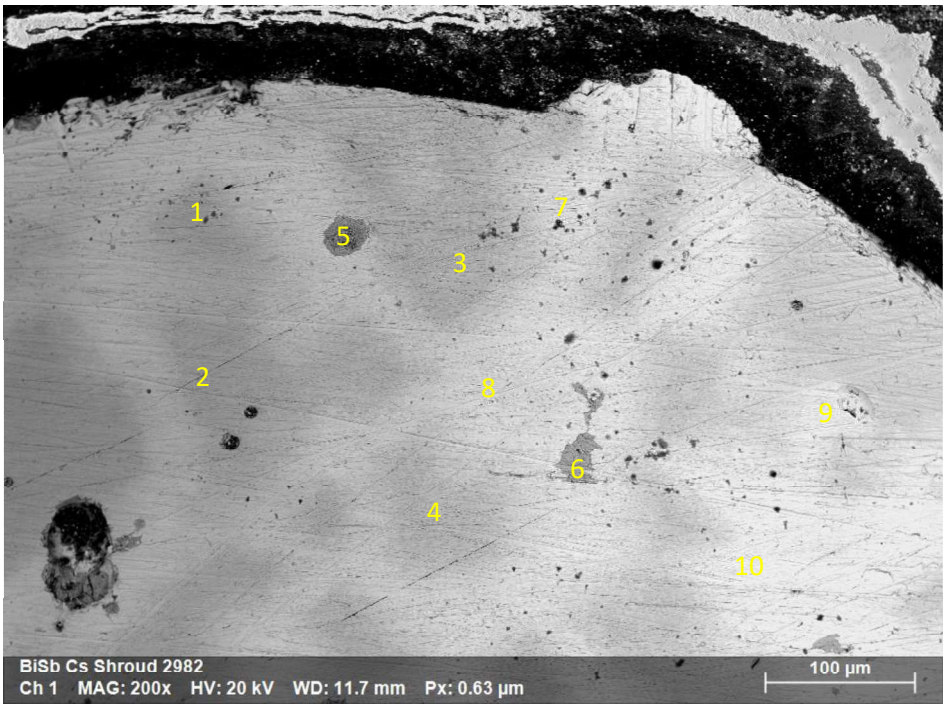

Figure 16. SEM-BSE photomicrograph from Figure 14b with marked locations for EDS analysis.

Table 3. Normalized concentration of elements (at. %) at locations on the Bi-Sb alloy electrode after the Cs-Bi/Sb-0 test, determined by EDS analysis at locations indicated in Figure 16.

Point Number	Antimony	Bismuth	Cesium
1	74.2	25.8	0
2	83.3	16.7	0
3	72.9	27.1	0
4	69.9	30.1	0
5	99.6	0	0
6	97.5	2.5	0
7	6.4	93.6	0
8	18.0	82.0	0
9	42.8	57.2	0
10	5.7	94.3	0

4.1.2 Cs/Sr-Bi/Sb-50

As discussed in Section 3.1.2, a short circuit is suspected to have occurred during test Cs/Sr-Bi/Sb-50, although an appreciable current was measured initially. In Figure 17, SEM-BSE photomicrographs of the alloy electrode/salt interface from test Cs/Sr-Bi/Sb-50 are shown. A magnified image of the portion of the salt-metal interface of the Bi-Sb alloy electrode outlined in red is shown. In this test 50 coulombs of charge were passed through the lithium depletion electrode prior to polarizing the liquid metal electrode. A total of ~120 coulombs of charge were passed through the alloy electrode before the current became anodic in this test.

The metal phase appears as a light grey and the dark grey is the salt phase, and are labeled on the images in Figure 17. At the left hand side of the low magnification image of the electrode, the boron nitride crucible can be seen and is marked on the image. In both images, slightly darker grey inclusions are seen in the metal phase that were not present in the alloy initially.

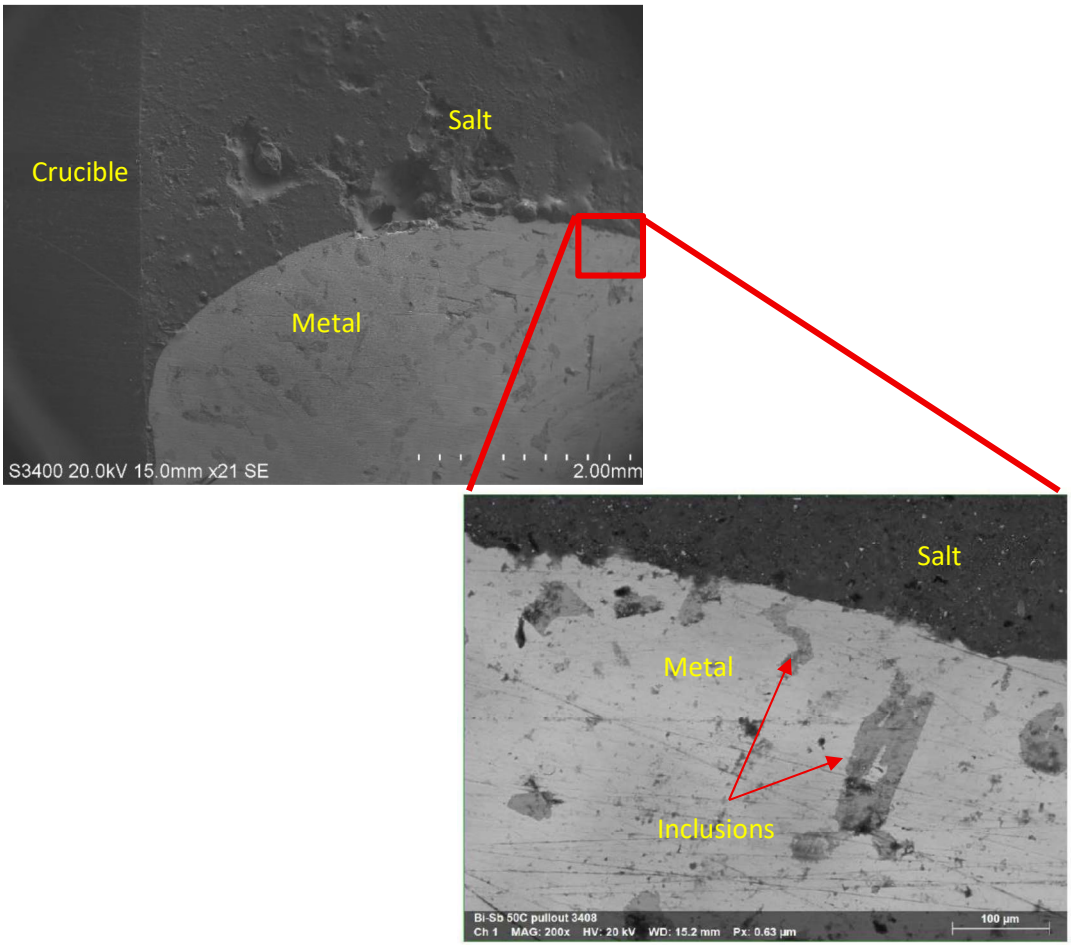

Figure 17. SEM-BSE photomicrograph of the Bi-Sb alloy electrode from the Cs/Sr-Bi/Sb-50 test, with a magnified image of the salt-metal interface

For the magnified region of the electrode imaged in Figure 17 outlined in red, EDS X-ray maps were generated to indicate the distribution of bismuth, antimony, chlorine, potassium, cesium and strontium near the salt-metal interface. Figure 18 shows these EDS maps. Light grey bismuth regions are distinict from dark grey antimony regions in the EDS X-ray maps as red and orange, respectively, in Figure 18. Strontium accumulated in the regions with dark contrast in the image. The cesium distribution is much more uniform with a band of slightly higher concentration at the salt-metal interface where there is also a higher concentration of antimony. Potassium and chlorine are detected in the salt phase. Isolated pockets of potassium align with anitmony-rich phases as well, indicating some co-deposition of potassium and strontium into the antimony as expected. The alloy electrode was liquid during deposition and therefore convective mixing likley occurred during deposition and as the alloy solidified post-test. This is the likely cause of these isolated pockets of antimony-rich phases containing potassium in the interior of the electrode.

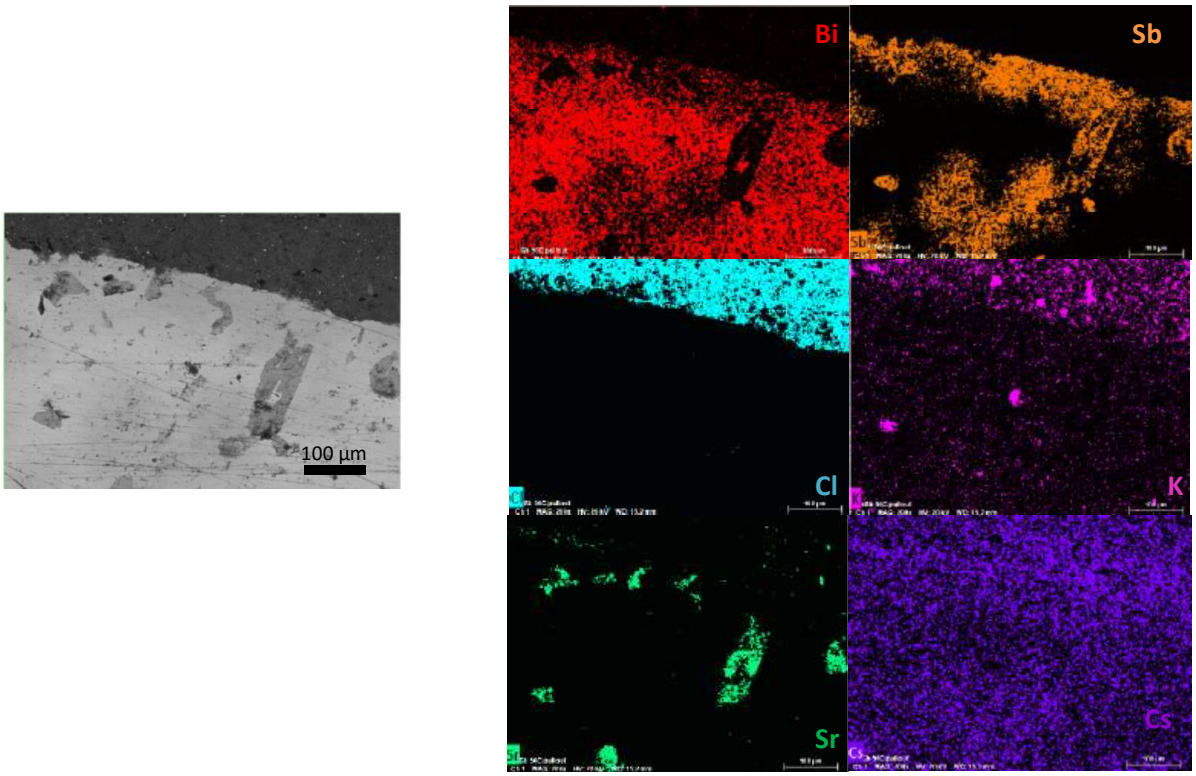

Figure 18. EDS X-ray maps of the magnified region imaged in Figure 17 of the Bi-Sb alloy electrode from the Cs/Sr-Bi/Sb-50 test analyzed for the presence of Bi, Sb, Cl, K Sr and Cs.

Figure 19 is a micrograph of the magnified image from Figure 18 where locations are marked for EDS analysis. Locations 1 and 2 are in the salt phase, locations 3-7 are in the metal alloy, and locations 8-11 are in dark contrast phases. The normalized concentrations of bismuth, antimony, potassium, chlorine, cesium, and strontium at these locations are shown in Table 4.

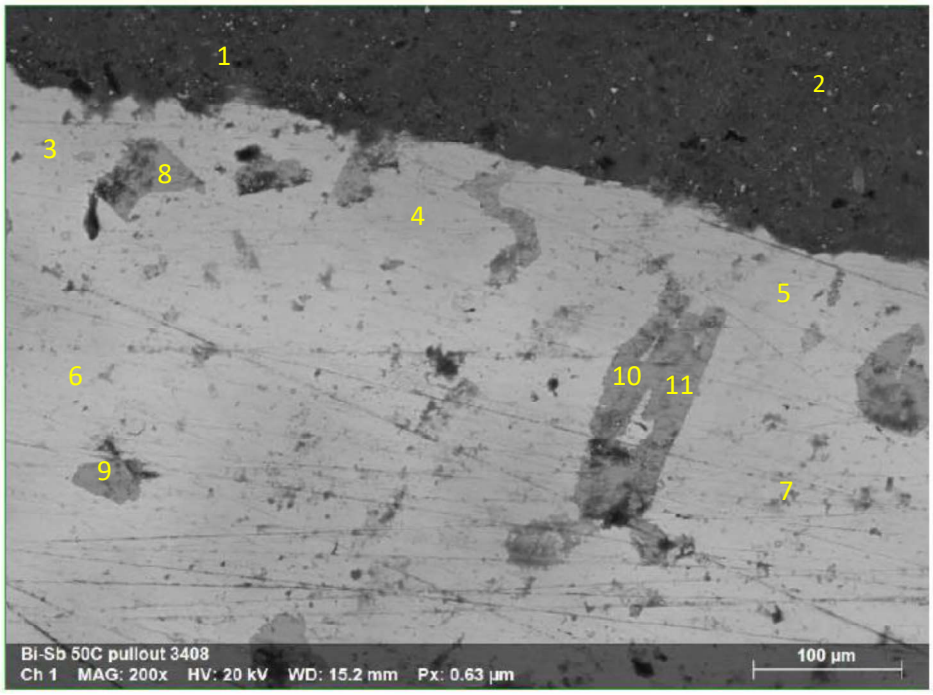

Figure 19. SEM-BSE photomicrograph of the magnified region imaged in Figure 17 with marked locations for EDS analysis

Cesium is detected in the salt phase at 3.9 - 5.2 at. % (locations 1 and 2), which is higher than the cesium concentration in the intial salt, which was 2.5 at. % Cs. This is consistent with local depletion of lithium increasing the local concentration of cesium in the salt due to the operation of the depletion electrode. Cesium is also detected at 1.8 - 4.0 at. % (locations 8-11) in the antimony-rich (bismuth content $\leq$ 1.5 at. %) phases indicating active metal deposition occurred. There is some chlorine detected at these locations as well, indicating there may be entrained salt near to the anitmony rich regions, however the concentration does not exceed the background level measured in the fresh alloy, seen in Table 2.

Strontium is detected in the anitmony rich phases at 3.9 - 5.2 at. % (locations 8-11) and in the salt phase at 1.7 at. %, at location 1. Strontium was present in the initial salt at 1.1 at. %. However, EDS point analyses are less sensitive to strontium than cesium, as determined during the analysis of an unreacted Bi-Sb alloy in Table 2 where in a sample devoid of strontium, as much as 1.3 at. % was detected.

Both cesium and strontium are exhibiting an affinity for antimony rich phases in both the X-ray maps and EDS point analyses, indicating that depositon into antimony may be more successful.

Table 4. Normalized concentrations of elements (at. %) at locations on the Bi-Sb alloy electrode after the Cs/Sr-Bi/Sb-50 test, determined by EDS analysis at locations indicated in Figure 19.

Concentration in atom %						
Point Number	Antimony	Bismuth	Cesium	Strontium	Chlorine	Potassium
1	0.7	0.1	5.2	1.7	87.1	5.2
2	0.0	0.1	3.9	0.0	90.1	5.9
3	69.9	30.1	0.0	0.0	0.0	0.0
4	84.2	13.0	0.0	1.8	1.0	0.0
5	71.4	28.6	0.0	0.0	0.0	0.0
6	10.8	89.2	0.0	0.0	0.0	0.0
7	61.4	38.6	0.0	0.0	0.0	0.0
8	80.8	1.0	3.2	5.1	7.3	2.6
9	82.6	1.4	4.0	3.9	4.5	3.6
10	82.2	1.2	3.8	4.1	5.3	3.4
11	82.0	1.5	1.8	5.2	7.7	1.8

Table 5 shows the normalized concentrations of the salt constituents in the electrolyte prior to and after active metal drawdown test Cs/Sr-Bi/Sb-50 calculated from the measured elemental concentrations in three samples of each salt. Averages and one standard deviation are reported for ease of comparison. The pre-test electrolyte was batched at 7 wt % CsCl (2.6 mol %) and 3 wt % $SrCl_2$ (2.2 mol %) and this concentration is shown in Table 5 for camparison. The average concentrations of CsCl and $SrCl_2$ in the post-test electrolyte are lower than those in the pre-test electrolyte, although the difference is within one standard deviation and neither is significantly different than the target as-batched composition.

Table 5. Normalized concentrations (mol %) of LiCl, KCl, CsCl and $SrCl_2$ in the electrolyte before and after the Cs/Sr-Bi/Sb-50 test calculated from the elemental concentrations measured by ICP-MS.

		Pre Test Samples					Post-Test Samples				
mol %	Target	Sample 1	Sample 2	Sample 3	Avg.	1s	Sample 1	Sample 2	Sample 3	Avg.	1s
LiCl	55.9	53.8	53.4	52.4	53.2	0.7	52.1	56.3	56.5	55.0	2.5
KCl	40.4	40.2	41.5	41.9	41.2	0.9	42.7	39.6	39.6	40.6	1.8
CsCl	2.6	3.9	3.4	3.7	3.7	0.3	3.5	2.8	2.8	3.0	0.4
$SrCl_2$	1.1	2.0	1.7	2.0	1.9	0.2	1.7	1.3	1.2	1.4	0.3

Table 6 shows the normalized concentration of metals measured in the dissolved half of the electrode alloy used in the Cs/Sr-Bi/Sb-50 test as measured by ICP-MS, compared to the target alloy composition (pre-test). Detectable levels of cesium and strontium are found in the alloy indicating that active metal deposition occurred.

Table 6. Normalized concentrations (mol %) of metals in the dissolved portion of the alloy electrode from the Cs/Sr-Bi/Sb-50 test as measured by ICP-MS.

mol %	Pre-test[a]	Post-Test	Uncertainty (10%)
Cs	-	0.36	0.04
Sr	-	1.39	0.14
Bi	50	49.09	4.91
Sb	50	49.16	4.92

[a] target composition, not measured

4.1.3 Cs/Sr-Bi/Sb-100

Figure 20 shows a BSE-SEM photomicrograph of the Bi-Sb alloy from the deposition test Cs/Sr-Bi/Sb-100 in which 100 coulombs of charge were passed to the lithium depletion electrode prior to deposition at the alloy electrode. In this test, a significantly smaller amount of charge was passed through the liquid metal alloy electrode (~30 coulombs) than in test Cs/Sr-Bi/Sb-50 (120 coulombs). Less charge passed corresponds to less deposition of the active metal, therefore we can expect a lower concentration of cesium and strontium in the liquid metal electrode upon analysis. The low currents and low charge passed through the electrode may indicate there was poor electrical connection to the liquid metal electrode during this test.

Additionally, the construction of the basket failed during the attempt to withdraw the electrode and the electrode remained immersed in the salt during cooling (~16 hours). This exposure to the salt

without polarization is likely to have resulted in the backreaction of deposited active metals with lithium and potassium in the salt, decreasing the recovery of active metals and increasing the co-deposition of lithium and potassium.

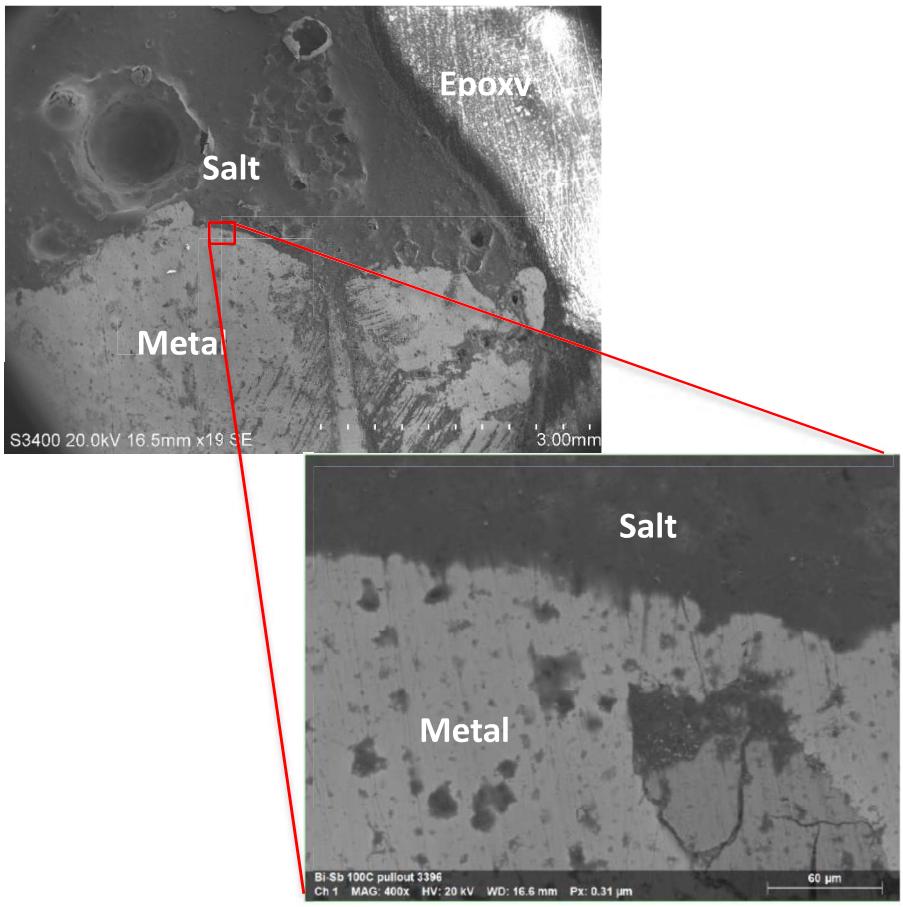

Figure 20. SEM-BSE photomicrograph of the Bi-Sb alloy electrode from the Cs/Sr-Bi/Sb-100 test

In Figure 20, the low magnification image of the electrode has a dark grey salt region in the top center and left containing several depressions, a light grey metallic region over the bottom third of the image and a bright region along the upper right-hand side which is the mounting epoxy. In the magnified image in Figure 20, the light grey region across the bottom two-thirds of the image is the metal phase with many dark grey inclusions and the very dark grey upper third of the image is the salt phase. A medium grey antimony-rich region is seen in the lower right-hand side of the metal phase.

For the magnified region of the electrode outlined in red in Figure 20, EDS X-ray maps indicating the distributions of bismuth, antimony, chlorinde, potassium, cesium and strontium near the salt-metal interface are shown in Figure 21.

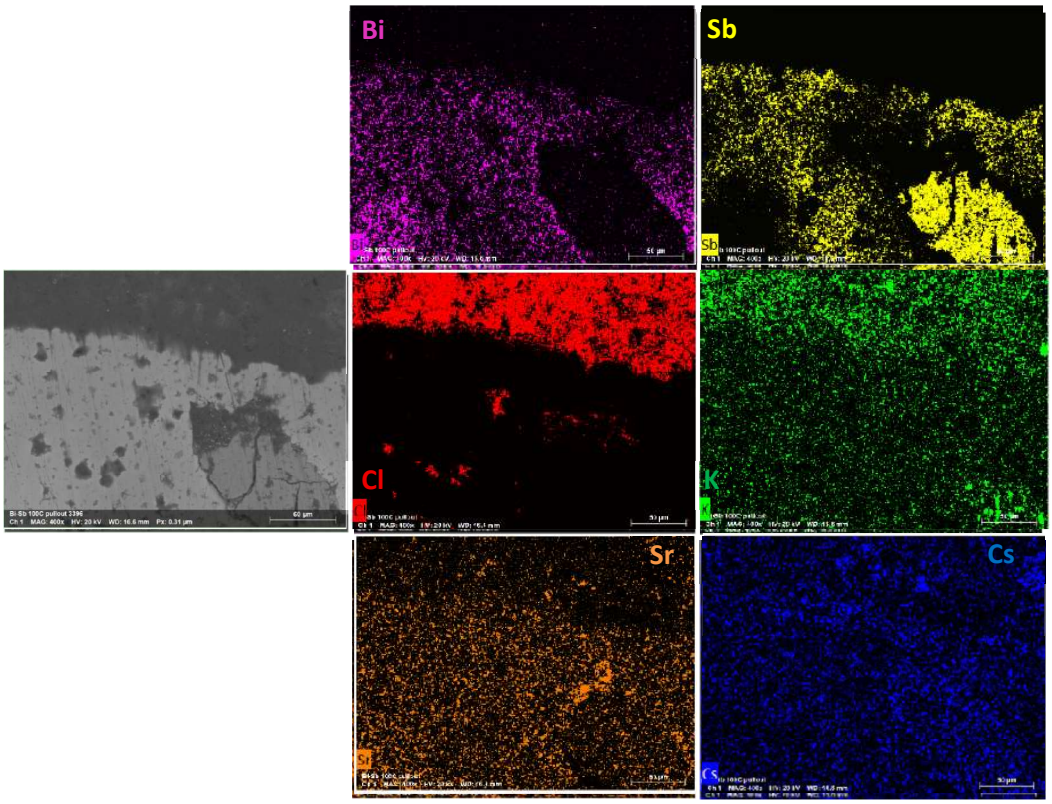

Figure 21. EDS X-ray maps of the magnified region imaged in Figure 20 of the Bi-Sb alloy electrode from the Cs/Sr-Bi/Sb-100 test, analyzed for the presence of Bi, Sb, Cl, K, Sr and Cs.

Bismuth and antimony are present in distinct regions in the X-ray maps of the metallic phase and not present in the salt phase. Chlorine is present in the salt phase and in several inclusions throughout the metal phase. Potassium is more concentrated in the salt phase and in the antimony-rich inclusion in the bottom right corner than in the rest of the metal phase. Strontium is more concentrated in the metallic phases than in the salt phase. Cesium shows a uniform signal across the whole sample not correlated to phases in the image, which is inconclusive.

Figure 22 is a micrograph of the magnified image from Figure 20 where locations are marked for EDS analysis. Locations 1-3 are in the salt phase and location 8 is a salt inclusion within the metal alloy. Locations 4-6 are in the metal phase at the salt-metal interface. Locations 7, 10 and 14 are in the sub-surface light grey metal phase and locations 9, 11 and 12 are in the antimony-rich medium grey metal phase. The normalized concentrations of bismuth, antimony, potassium, chlorine, cesium, and strontium at these locations are shown in Table 7.

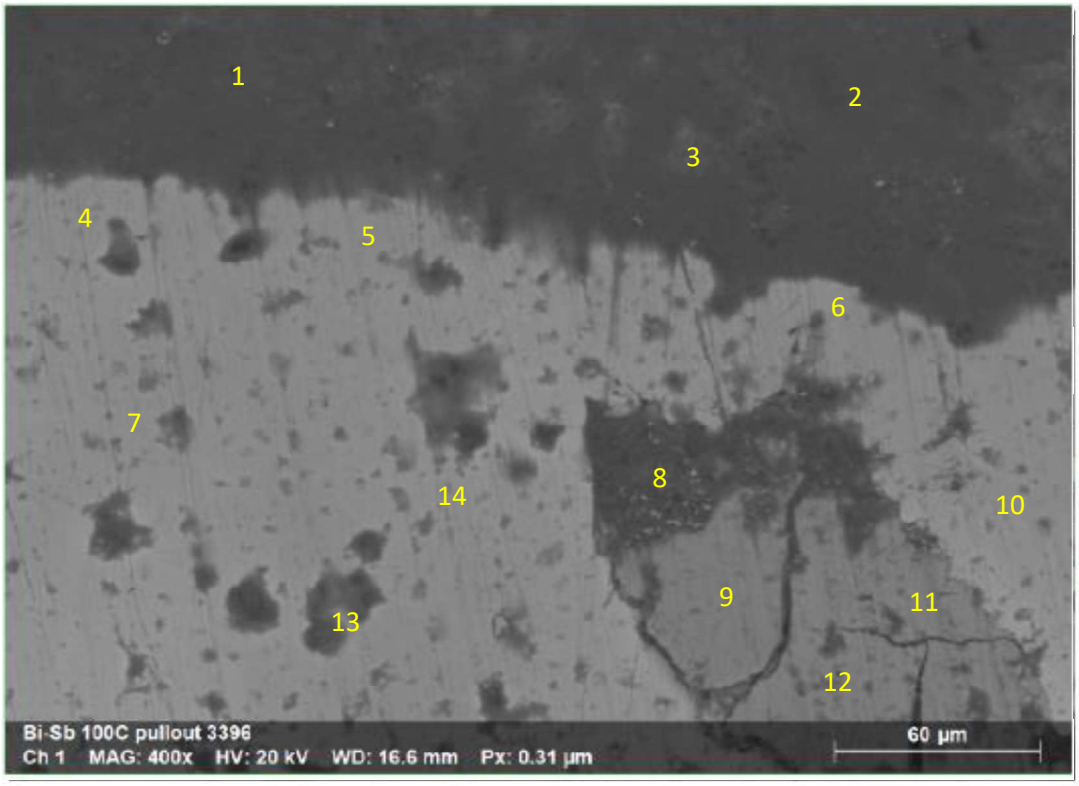

Figure 22. SEM-BSE photomicrograph of magnified region imaged in Figure 20 with marked locations for EDS analysis.

Spot analyses locations 1-3 in the salt phase show concentrations of cesium (4.2 - 9.3 at. %) higher than present in the salt initially (2.5 at. %), and an erichment in chlorine. Indicating the depletion of lithium in the local area of the electrode was successful. Locations 4-6 in the metal phase at the salt-metal interface indicate the region is devoid of active metals. This indicates that either little or no active metals were deposited due to poor electrical connections, or active metals at the interface backreacted with lithium and potassium in the salt during cooling, or both.

No cesium or strontium is detected in EDS analysis of locations deeper into the electrode (7, 10, and 14), which are less enriched in antimony. This is expected as the product of test Cs/Sr-Bi/Sb-50, analyzed in Table 4, showed that cesium is only detected in antimony rich phases.

Locations 8 and 13 are salt inclusions. Locations 9, 11 and 12 are antimony rich with very low bismuth concentrations (< 2.6 at. %) and contain measurable amounts of cesium (0.5 - 3.0 at. %). The detection of cesium in the interior far from the interface indicates that active metal deposition occurred and the lack of active metals in the surface regions (locations 4 - 6) of the metal is due to backreaction with lithium in the salt during cooling. There is notable chlorine content in locations 9, 11 and 12 as well (7.5 - 25 at. %) indicating that there may be salt occluded in the antimony rich region.

Table 7. Normalized concentrations of elements (at. %) at locations on the Bi-Sb alloy electrode after the Cs/Sr-Bi/Sb-100 test, determined by EDS analysis at locations indicated in Figure 22.

Concentration in atom %						
Point Number	Antimony	Bismuth	Cesium	Strontium	Chlorine	Potassium
1	0.4	0.5	4.2	1.1	86.9	6.9
2	0	0.6	8.0	0	85.2	6.2
3	0	0.1	9.3	1.0	86.4	3.2
4	85.7	14.3	0	0	0	0
5	89.4	10.6	0	0	0	0
6	89.7	9.2	0	0	1.1	0
7	79.6	20.4	0	0	0.0	0
8	4.7	2.7	7.8	2.2	80.1	2.5
9	86.7	0.4	1.9	0.2	9.7	1.1
10	78.1	21.9	0	0	0	0
11	90.1	1.5	0.5	0	7.5	0.4
12	66.2	2.6	3.0	0.9	25.4	1.9
13	42.0	10.0	0	0	48.0	0
14	77.5	22.5	0	0	0	0

Table 8 shows the normalized concentrations of the salt constituents in the electrolyte prior to and after active metal drawdown test Cs/Sr-Bi/Sb-100 calculated from the measured elemental concentrations in three samples of each salt. Averages and one standard deviation are reported for ease of comparison. The pre-test electrolyte was batched at 7 wt % CsCl (2.6 mol %) and 3 wt % $SrCl_2$ (2.2 mol %) and this concentration is shown in Table 8 for camparison. The average concentrations of CsCl and $SrCl_2$ in the post-test electrolyte are within one standard deviation of the concentrations in the pre-test electrolyte and are not significanlty different from the target electrlolyte composition.

Table 8. Normalized concentrations (mol %) of LiCl, KCl, CsCl and $SrCl_2$ in the electrolyte before and after the Cs/Sr-Bi/Sb-100 test calculated from the elemental concentrations measured by ICP-MS.

		Pre Test Samples					Post-Test Samples				
mol %	Target	Sample 1	Sample 2	Sample 3	Avg.	1s	Sample 1	Sample 2	Sample 3	Avg.	1s
LiCl	55.9	54.0	52.8	60.0	55.6	3.8	56.9	59.1	54.8	56.9	2.1
KCl	40.4	41.5	41.3	38.2	40.3	1.8	39.5	38.0	41.0	39.5	1.5
CsCl	2.6	2.9	3.9	1.4	2.7	1.2	2.5	2.1	2.9	2.5	0.4
$SrCl_2$	1.1	1.6	2.0	0.4	1.3	0.8	1.1	0.9	1.3	1.1	0.2

Table 9 shows the normalized concentration of metals measured in the dissolved half of the alloy produced in the Cs/Sr-Bi/Sb-100 test as measured by ICP-MS, compared to the target alloy composition (pre-test). Detectable levels of cesium and strontium are found in the alloy indicating that active metal deposition occurred.

Table 9. Normalized concentrations (mol %) of metals in the dissolved portion of the alloy electrode from the Cs/Sr-Bi/Sb-100 test as measured by ICP-MS.

Mol %	Pre-test[a]	Post-Test	Uncertainty (10%)
Cs	-	0.12	0.01
Sr	-	0.79	0.08
Bi	50	45.06	4.51
Sb	50	54.03	5.40

[a] target composition, not measured

The alloy from the Cs/Sr-Bi/Sb-50 test (see Table 6) contained three times as much cesium and nearly twice as much strontium as the alloy from the Cs/Sr-Bi/Sb-100 test. This was expected because the amount of charge passed to the liquid metal electrode in the Cs/Sr-Bi/Sb-50 test (120 coulombs) was four times that in the Cs/Sr-Bi/SB-100 test (30 coulombs).

4.2 Analysis of an Electrode from Deposition Tests into an Antimony Electrode

4.2.1 Cs/Sr-Sb-2

Figure 23 shows a photomicrograph of the antimony electrode from deposition test Cs/Sr-Sb-2 into pure antimony using a lithium depletion electrode constructed from brass. In this test, 100 coulombs of charge were passed through the lithium depletion electrode in just 500 s. Current at the deposition electrode was very low and only ~5 coulombs of charge were passed through the antimony electrode over the duration of the test, ~3000 s.

In the micrograph in Figure 23 the electrode does not appear to have melted in the test, as evidenced by its non-uniform shape within the crucible. The Bi-Sb electrodes seen in Section 4.1 take the shape of the crucible on three sides as expected for a liquid in a container. In Figure 23, there is salt alongside and under portions of the antimony electrode. It is suspected that the electrode did not reach an internal temperature of 650 °C and therefore remained solid during the test.

Despite this, in the magnified image in Figure 23 of the salt-metal interface dark inclusions are observed in the light grey metal phase, and lighter phases are observed in the dark grey salt phase. These inclusions were analyzed using EDS.

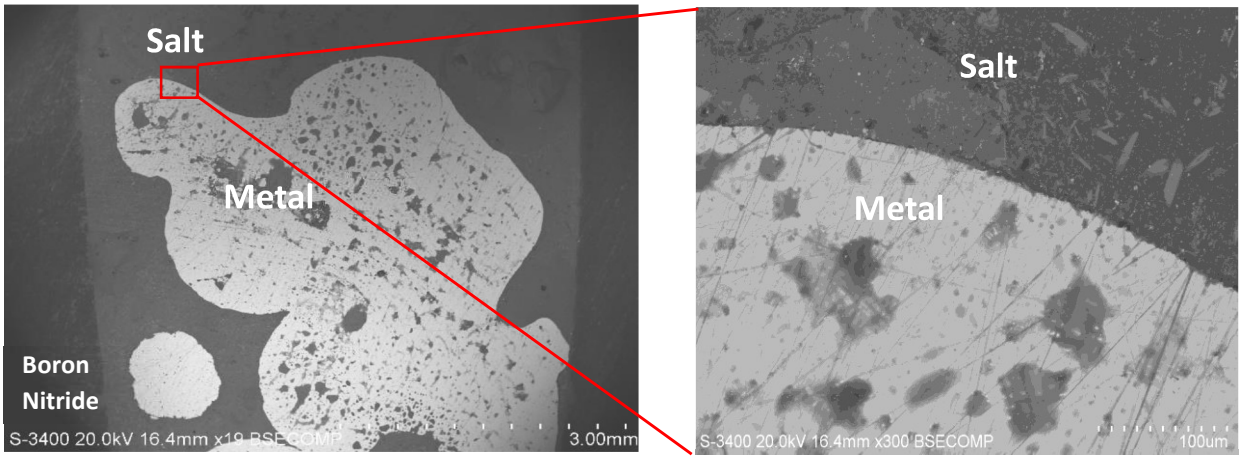

Figure 23. SEM-BSE photomicrographs of the antimony electrode from the deposition test Cs/Sr-Sb-2.

Figure 24 shows EDS X-ray maps of the magnified image of the salt-metal interface of the antimony electrode in Figure 23. No antimony is detected in the salt phase as expected, however salt inclusions are found throughout the metal phase. The light grey regions within the salt phase appear to be concentrated in strontium. Potassium is more concentrated in the salt phase, but is not found in the dark grey inclusions in the alloy. Cesium is detected uniformaly across a majority of the sample, including in a half circle of salt at the salt-metal interface in the upper left of the image. This same half circle in the salt is enriched in potassium. It appears deposition of active metals did not occur, because the electrode remained a solid.

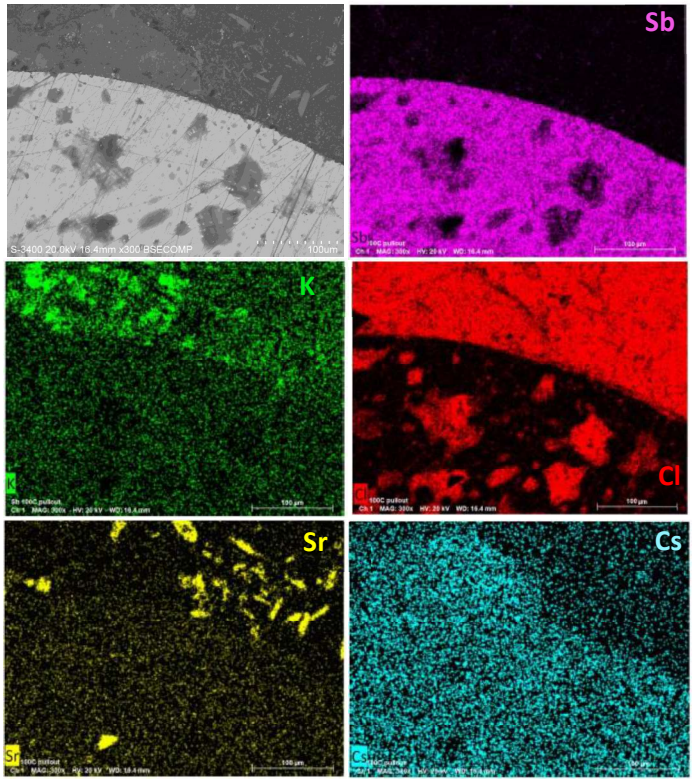

Figure 24. EDS X-ray maps of antimony electrode from the deposition test Cs/Sr-Sb-2, analyzed for the presence of Sb, Cl, K, Sr, and Cs.

5. CONCLUSIONS AND RECOMMENDATIONS

The use of a lithium depletion electrode to improve recovery of active metals from pyroprocessing salts by electrodeposition into liquid metals was assessed by comparing chronocoulometric data and SEM analyses of alloys generated during the simultaneous depletion and deposition test (Cs-Bi/Sb-0) and during tests with 50 (Cs/Sr-Bi/Sb-50) and 100 (Cs/Sr-Bi/Sb-100) coulombs of lithium depletion prior to deposition of active metals. The test with lithium depletion of 50 coulombs prior to deposition into liquid metals, Cs/Sr-Bi/Sb-50, generated local cesium concentrations of 3 - 5 at. % in point analyses of antimony-rich regions of the alloy electrode and 0.36 mol % cesium was measured in the bulk alloy, which is above the cesium detected in the simultaneous depletion and deposition test (Cs-Bi/Sb-0) and above the salt concentration of 2.5 at. % cesium. No reduction in cesium concentration in the bulk salt was measured.

Bulk analysis of the alloy electrode showed three times as much cesium in the Cs/Sr-Bi/Sb-50 test (0.36 mol %) which had ~120 coulombs passed to it during deposition than in the Cs/Sr-Bi/Sb-100 test (0.12 mol % Cs) which had ~30 coulombs passed to it during deposition. Concentration of active metal in the liquid metal electrode correlates, as expected, with the amount of charge passed. And the charge passed is a function of the current achievable at the electrode. The currents at the mesh lithium depletion electrodes were invariably larger than the currents at liquid metal electrodes, as expected due to the difference in surface area between mesh electrodes and liquid metal electrodes, whose surface is limited to the circular surface of the pool of liquid metal. For this method to be feasible it will likely be necessary to increase the ratio of the surface area of the liquid metal electrode to the salt volume and thereby increase the achievable current at the electrode and associated deposition of active metals. In subsequent tests, the electrode surface area to salt volume ratio will be increased to demonstrate the effectiveness of removing active metals from pyroprocessing salt by electrodeposition by producing a measurable decrease in active metal concentrations in surrogate pyroprocessing salts.

Backreaction of active metals with lithium in the salt occurred in two tests (Cs/Sr-Bi/Sb-100 and Cs/Sr-Sb-1) where a failure in the lithium depletion electrode construction prevented immediate removal of the electrodes from the salt prior to cooling. During Cs/Sr-Bi/SB-100, cesium was detected within the alloy by SEM, but not in regions at the salt-metal interface. This is consistent with the hypothesis that active metals were deposited and those at the surface backreacted with the lithium and potassium in the salt during cooling. Therefore, lithium depletion and active metal deposition electrodes should be designed to ensure they can reliably be removed from the salt post-test for cooling. Further analysis of the electrical behavior of the lithium depletion electrode and its composition after use may provide insights into appropriate sizing or lifetime of this component.

In all tests using Bi-Sb alloys, cesium and strontium preferentially accumulated in antimony-rich regions. Deposition into pure antimony is expected to be more efficient. Tests conducted here with

antimony electrodes did not achieve a liquid state antimony electrode and therefore should be repeated at a higher temperature to demonstrate that this electrode material will be more effective.

Application of this method of recovering active metals to the pyroprocessing flowsheet poses an additional technical challenge. Salts will be deficient in lithium due to the use of the lithium depletion electrode. Methods of chlorinating the lithium on the depletion electrode to return it to the salt or adding LiCl to the salt should be identified and assessed to close the pyroprocessing flowsheet. In addition, the suitability of the generated active-metal electrodes for disposal needs to be assessed.

REFERENCES

M.A. Rose and S. Thomas. (2023). “Management of Alkali and Alkaline Earth Fission Products in Used Pyroprocessing Salt”. Argonne National Laboratory report ANL/CFCT-23/20.

Nigl, Lichtenstein, Kong and Kim. (2020). “Electrochemical Separation of Alkaline-Earth Elements from Molten Salts Using Liquid Metal Electrodes”. *ACS Sustainable Chem. Eng*. 8, 14818-14824.

T. Lichtenstein, J. Gesualdi, L. Gardner and M.A. Rose. “Cesium Removal from Surrogate Pyroprocessing Salt by Electrodeposition”. Argonne National Laboratory report ANL/CFCT-24/13. June 2024

W. Gąsior and Z. Moser. (2001). “Thermodynamic Study of Liquid Lithium-Lead Alloys Using the EMF Method”. *J. Nuc. Mater. 294*, 77-83.

Petric, A., Pelton, A.D., Saboungi, M.-L. (1988). "Thermodynamic properties of liquid K-Bi alloys by electromotive force measurements" *J. Phys. F. Met. Phys. 18* 1473–1489.

H. Okamoto. (2012). “Supplemental Literature Review: Section III: Bi-Sb (Bismuth-Antimony)”. *J. Phase Equilib. Diffus*. 33 (6), 492.

Chemical and Fuel Cycle Technologies Division
Argonne National Laboratory
9700 South Cass Avenue, Bldg. 205

Lemont, IL 60439

www.anl.gov

Argonne National Laboratory is a U.S. Department of Energy laboratory managed by UChicago Argonne, LLC